Possible chiral spin liquid state in the $S = 1/2$ kagome Heisenberg model

Rong-Yang Sun,[1,2,3,*] Hui-Ke Jin,[4,*] Hong-Hao Tu,[5,†] and Yi Zhou[6,7,3,8,‡]

[1]*Computational Materials Science Research Team, RIKEN Center for Computational Science (R-CCS), Kobe, Hyogo, 650-0047, Japan*
[2]*Quantum Computational Science Research Team, RIKEN Center for Quantum Computing (RQC), Wako, Saitama, 351-0198, Japan*
[3]*Kavli Institute for Theoretical Sciences, University of Chinese Academy of Sciences, Beijing 100190, China*
[4]*Department of Physics TQM, Technische Universität München, James-Franck-Straße 1, D-85748 Garching, Germany*
[5]*Institut für Theoretische Physik, Technische Universität Dresden, 01062 Dresden, Germany*
[6]*Institute of Physics, Chinese Academy of Sciences, Beijing 100190, China*
[7]*Songshan Lake Materials Laboratory, Dongguan, Guangdong 523808, China*
[8]*CAS Center for Excellence in Topological Quantum Computation, University of Chinese Academy of Sciences, Beijing 100190, China*

(Dated: March 25, 2022)

The nature of the ground state for the $S = 1/2$ kagome Heisenberg antiferromagnet (KHAF) has been elusive. We revisit this challenging problem and provide numerical evidence that its ground state might be a chiral spin liquid. Combining the density matrix renormalization group method and analytical analyses, we demonstrate that the previously observed chiral spin liquid phase in the KHAF with longer-range couplings is stable in a broader region. We characterize the nature of the ground state by computing energy derivatives, revealing ground-state degeneracy arising from spontaneous breaking of time-reversal symmetry, and targeting the semion sector. We further investigate the phase diagram in the vicinity of the KHAF and observe a $\sqrt{3}\times\sqrt{3}$ magnetically ordered phase and two valence-bond crystal phases.

Introduction. The search of quantum spin liquids (QSLs) has been an active endeavour in condensed matter physics for decades [1–8]. In contrast to magnetically ordered states that are characterized by spontaneous symmetry breaking and local order parameters, this novel state of matter manifests itself in other exotic ways, such as long-range quantum entanglement and fractional spin excitations. In particular, a gapped QSL must be associated with a non-trivial topological order [9, 10]. Chiral spin liquid (CSL) is defined as a topological QSL that breaks time-reversal symmetry (TRS) and parity symmetry. It was first proposed by Kalmeyer and Laughlin [11, 12] that the bosonic fractional quantum Hall state at filling factor $\nu = 1/2$ might be the ground state of some frustrated Heisenberg antiferromagnets in two dimensions. Soon after that, Wen, Wilczek, and Zee [13] introduced spin chirality $E_{123} \equiv \mathbf{S}_1 \cdot (\mathbf{S}_2 \times \mathbf{S}_3)$ to characterize such a TRS breaking QSL state, which names CSL.

With strong geometric frustration and concrete material realizations, the $S = 1/2$ kagome Heisenberg antiferromagnet (KHAF) has been regarded as one of the promising candidates hosting QSLs [14–18]. Theoretically, it has been generally accepted that the ground state of the KHAF with nearest-neighbor (NN) interactions is a QSL state [6, 18], although a valence-bond crystal (VBC) with a 36-site unit cell was proposed as well [19–22]. However, despite extensive exploring [23–47], the nature of the QSL state is still a puzzle. Above all, the issue of "to gap or not to gap" has not yet been settled down unambiguously. While exact diagonalization [24–30], density matrix renormalization group (DMRG) [32–36], and a tensor network variational calculation [37] indicate a finite energy gap, variational Monte Carlo [38–41], infinite DMRG [42], and further tensor network studies [43, 44] favor a gapless ground state, i.e., the U(1) Dirac QSL [38].

Meanwhile, some early mean-field calculations proposed the possibility of a CSL [19, 48–50]. Further studies have shown that a CSL can be stabilized by the KHAF with chiral three-spin interactions [51, 52] or with 2nd and 3rd NN Ising [53] or Heisenberg couplings [52, 54–56], where the nature of this CSL was found to be of the $\nu = 1/2$ Kalmeyer-Laughlin type.

In this Letter, we reexamine the evolution of the ground state of the KHAF with equal 2nd and 3rd NN Heisenberg couplings. We use the DMRG method [57–59] (up to bond dimension $D = 8000$) and analytical analyses to map out its ground-state phase diagram [see Fig. 1(a)], which consists of a $\sqrt{3}\times\sqrt{3}$ ordered phase, two distinct VBC phases, and a CSL phase. The most striking observation is that the ground state of the KHAF with only NN interactions lies in the aforementioned CSL phase, which is supported by the calculations of energy susceptibility, wave function fidelity, and ground-state degeneracy. It is further shown that the CSL phase extends to the region where 2nd and 3nd NN couplings are ferromagnetic.

Model. We consider the KHAF with SU(2)-symmetric longer-range couplings (referred to as the J-J' model hereafter)

$$H = J \sum_{\langle ij\rangle_1} \mathbf{S}_i \cdot \mathbf{S}_j + J' \left(\sum_{\langle ij\rangle_2} \mathbf{S}_i \cdot \mathbf{S}_j + \sum_{\langle ij\rangle_3} \mathbf{S}_i \cdot \mathbf{S}_j \right), \qquad (1)$$

where $\langle ij\rangle_\gamma$ ($\gamma = 1, 2, 3$) denote the γ-th NN bonds on the kagome lattice (the 3rd NN bonds are defined within hexagons only). Henceforth we set $J = 1$ as the energy unit and focus on the regime of $-0.15 \leq J' \leq 0.4$ in the YC cylinder geometry [see Fig. 1(b)].

Chiral spin liquid phase. Let us start the discussion of Eq. (1) from its relatively well understood CSL phase with moderately large $J' \gtrsim 0.08$ [54, 55], for which much insight can be gained from a Gutzwiller projected wave func-

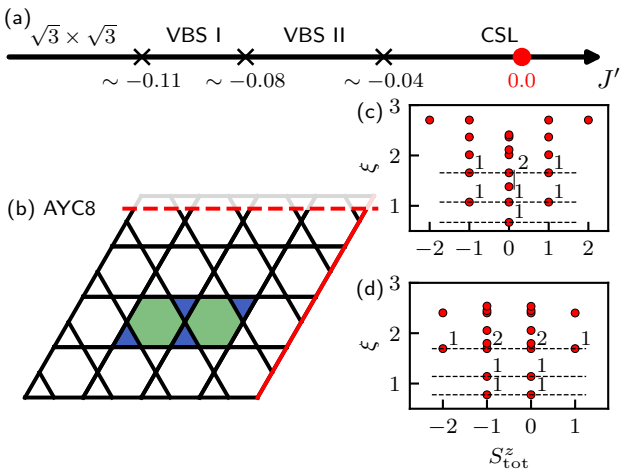

FIG. 1. (a) The phase diagram of the J-J' model consisting of a $\sqrt{3}\times\sqrt{3}$ ordered phase, two VBC phases [VBC I and VBC II with different patterns, see Figs. 3(e) and (f)], and a CSL phase. Note that the KHAF at $J'=0$ (red dot) also lies in the CSL phase. (b) YC8 cylinder for the kagome lattice, where the dashed red line represents periodic boundary condition, and the flat right edge is highlighted by the solid red line. The colored area denotes a unit cell of the $[\frac{\pi}{2},0]$ mean-field ansatz, with $\pi/2$ (zero) flux through the elementary triangles (hexagons). (c), (d) Entanglement spectra for ground states in the (c) identity and (d) semion sectors with $J'=0.4$.

tion [52, 56]. This wave function is constructed in a fermionic parton representation for $S=1/2$ spins, $S^a_i=\frac{1}{2}\boldsymbol{c}^\dagger_i\sigma^a\boldsymbol{c}_i$ ($a=x,y,z$), where σ^a are Pauli matrices and $\boldsymbol{c}_i=(c_{i,\uparrow},c_{i,\downarrow})$ are fermion annihilation operators. The physical Hilbert space of $S=1/2$ is restored by imposing a local single-occupancy constraint $\sum_{\sigma=\uparrow,\downarrow}c^\dagger_{i\sigma}c_{i\sigma}=1$.

In the parton representation, a mean-field Hamiltonian, parameterized by link variables $\chi_{ij}=e^{\phi_{ij}}$ on the 1st NN bonds, takes the form of [38]

$$H_{\rm MF}=\sum_{\langle ij\rangle_1}\sum_{\sigma=\uparrow,\downarrow}(\chi_{ij}c^\dagger_{i\sigma}c_{j\sigma}+\text{H.c.})\,. \tag{2}$$

Due to the SU(2) gauge redundancy [60–63], Gutzwiller projected states obtained from Eq. (2) are distinguished by the gauge fluxes threading through elementary triangles and hexagons on the kagome lattice [see Fig. 1(b)]. A CSL state is of particular interest that corresponds to the ansatz with $\frac{\pi}{2}$-flux through triangles and zero-flux through hexagons, dubbed as $[\frac{\pi}{2},0]$ state [64].

With a cylindrical boundary condition, the $[\frac{\pi}{2},0]$ state exhibits four exact boundary zero modes, $d^\dagger_{L\sigma}$ and $d^\dagger_{R\sigma}$, where L (R) denotes the left (right) boundary of the cylinder. For the CSL state, the minimally entangled states (anyon eigenbasis) [65] are constructed as follows [66, 67]:

$$|\Psi_1\rangle=\hat{P}_G d^\dagger_{L\uparrow}d^\dagger_{L\downarrow}|\Phi\rangle,\quad |\Psi_2\rangle=\hat{P}_G d^\dagger_{L\uparrow}d^\dagger_{R\downarrow}|\Phi\rangle\,, \tag{3}$$

where $|\Phi\rangle$ is a Fermi sea state with all negative energy modes of Eq. (2) being occupied, and $\hat{P}_G$ is the Gutzwiller projection operator imposing the single-occupancy constraint. With the MPO-MPS method [67, 68], the CSL anyon eigenbasis in Eq. (3) can be converted into matrix product states (MPSs) with high fidelity.

For the J-J' model in the CSL phase, two topologically degenerate ground states, denoted by $|\Psi_{\rm I}\rangle$ ($|\Psi_{\rm S}\rangle$) in the identity (semion) sector, can be obtained by initializing DMRG with their parton counterpart $|\Psi_1\rangle$ ($|\Psi_2\rangle$) [69, 70]. For a YC8 cylinder with 152 sites, the ground-state energy difference between two topological sectors is $\Delta E_0\approx 0.33$ (0.27) for $J'=0.4$ (0.2), and the two ground states are orthogonal to each other, as indicated by their overlap $|\langle\Psi_{\rm I}|\Psi_{\rm S}\rangle|\sim 10^{-11}$ (10^{-9}). We note that the time-reversal partner of $|\Psi_{\rm I}\rangle$ ($|\Psi_{\rm S}\rangle$), denoted by $|\Psi_{\rm I}{}^*\rangle$ ($|\Psi_{\rm S}{}^*\rangle$), has the same energy as $|\Psi_{\rm I}\rangle$ ($|\Psi_{\rm S}\rangle$) due to the spontaneous TRS breaking. As shown in Figs. 1(c) and (d), the entanglement spectrum [71, 72] of $|\Psi_{\rm I}\rangle$ ($|\Psi_{\rm S}\rangle$) displays the characteristic counting $\{1,3,4,(7),...\}$ ($\{2,2,6,(8),...\}$), which suggests the chiral $\mathrm{SU}(2)_1$ Wess-Zumino-Witten model being the edge conformal field theory. These results firmly validate the existence of a CSL phase of Kalmeyer-Laughlin type in this model.

Spontaneous TRS breaking at $J'=0$. After examining the CSL phase at relatively large J', we now show that this CSL phase is adiabatically connected to the ground state at $J'=0$ point. For this purpose, we carry out DMRG calculations that are initialized with randomly-generated MPSs (dubbed as Random-DMRG) as well as specific wave functions (dubbed as Boosted-DMRG [69]). For Boosted-DMRG, we adopt either the parton ansatz (3) or post-optimized MPSs of the neighborhood Hamiltonian in parameter space (see also a related adiabatic DMRG approach [54, 73]). Nevertheless, the ground-state energies obtained by Random- and Boosted-DMRG are almost identical [74], both of which agree with the results in Ref. [55]. For the KHAF with $J'=0$, the ground-state energy per site is found to be $-0.4383(6)$, which also agrees with the best available DMRG results [33, 34].

For $-0.15\le J'\le 0.4$, the first-order derivative of the ground-state energy E_0 does not show any singularities, as shown in Fig. 2(a). However, we observe that the second-order derivative of E_0 exhibits three sharp peaks [see Fig. 2(a)]. The location of these peaks indicates that there is no (at least neither first nor second-order) phase transition within the region of $0\le J'\le 0.1$. In contrast, previous DMRG studies [54, 55] suggest a critical point at $J'_c\approx 0.08$ that is identified by vanishing spin chirality. This contradiction can be resolved as follows [74]: Consider the spin chirality $\chi_{ijk}(\ge 0)$ defined on an elementary triangle $\triangle_{ijk}$ [see Fig. 1(b)], we find that (i) χ_{ijk} is sizable for a state deep inside the CSL phase, e.g., $\chi_{ijk}\sim 0.06$ at $J'=0.2$; (ii) χ_{ijk} will decrease rapidly as J' decreases and exceed $J'=0.1$, i.e., $\chi_{ijk}\sim 6\times 10^{-4}$ at $J'=0.08$, which is small but does not vanish numerically; (iii) χ_{ijk} continues to decrease to a numerical zero, $\chi_{ijk}\sim 6\times 10^{-7}$ at $J'=-0.04$, around which CSL to VBC II phase transition occurs [see Figs. 1(a) and 2].

In addition to the energetics, we have also calculated the wave function fidelity $F(J')=|\langle\Psi(J')|\Psi(J'-\Delta J')\rangle|$ and the corresponding susceptibility $\chi_F\equiv \mathrm{d}F/\mathrm{d}J'$, where $|\Psi(J')\rangle$ is

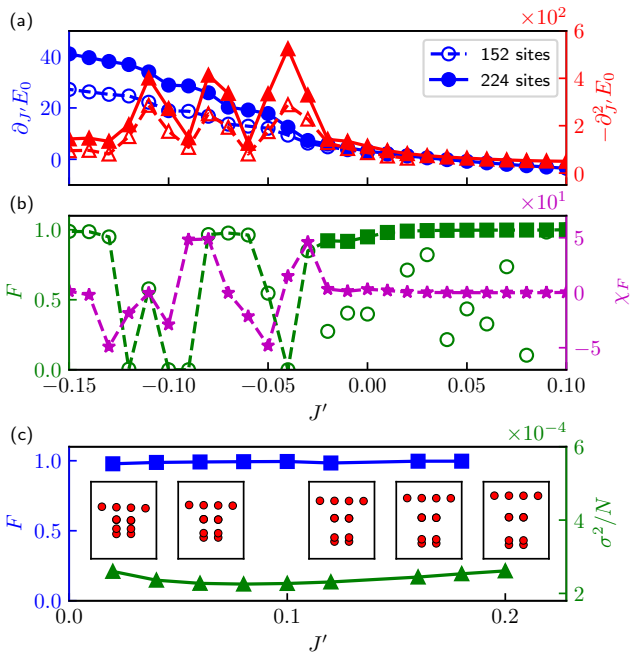

FIG. 2. (a) The first- and second-order derivatives of the ground-state energy E_0 versus J'. The empty and full markers with dashed and solid lines stand for the data obtained on 152- and 224-site YC8 cylinders, respectively. (b) The neighboring wave function overlap $\langle\Psi(J')|\Psi(J'-\Delta J')\rangle$ ($\Delta J' = 0.01$) and the corresponding susceptibility versus J'. The empty circles are obtained by Random-DMRG, and the full squares are obtained by Boosted-DMRG. (c) Neighboring wave functions overlaps (blue squares), energy variances (green triangles), and the low entanglement spectra (thumbnails) of semion-sector ground states in 152-site YC8 cylinders obtained by Boosted-DMRG.

the ground state obtained by Random- or Boosted-DMRG initialized with $|\Psi(J'+\Delta J')\rangle$. Here we adopt $\Delta J' = 0.01$. For $J' \leq -0.04$, the kinks in F and singularities in χ_F, as shown in Fig. 2(b), are in agreement with the location of the sharp peaks in the second-order derivative of E_0.

For $-0.03 < J' \leq 0.09$, the fidelity F obtained from Random-DMRG (using *real* MPSs) fluctuates strongly without any regular pattern. This seemingly odd result indicates that the system either has degenerate ground states (from which DMRG chooses their superposition, which varies randomly at different J') or hosts a pile of phase transitions within this narrow region. As we mentioned earlier, $|\Psi_\mathrm{I}\rangle$ and its time-reversal partner $|\Psi_\mathrm{I}{}^*\rangle$ are Kramers degenerate ground states in the CSL phase, whose *real* combinations are $|\Phi_\mathrm{I}\rangle = (|\Psi_\mathrm{I}\rangle + |\Psi_\mathrm{I}{}^*\rangle)/\sqrt{2}$ and $|\tilde{\Phi}_\mathrm{I}\rangle = i(|\Psi_\mathrm{I}\rangle - |\Psi_\mathrm{I}{}^*\rangle)/\sqrt{2}$. As usual, Random-DMRG using real MPSs would find their superposition $\cos(\theta)|\Phi_\mathrm{I}\rangle + \sin(\theta)|\tilde{\Phi}_\mathrm{I}\rangle$ [75], where θ is not under control and varies with J'. This would lead to a fluctuating fidelity F in Fig. 2(b). Furthermore, we note that θ can be fixed (or slowly varying) by performing a series of Boosted-DMRG calculations, i.e., the ground-state search for coupling J' is carried out by initializing DMRG with the post-optimized MPS for coupling $J' + \Delta J'$. This adiabatic procedure can be done recursively from $J' = 0.1$ to $J' = -0.03$ and, indeed, the fidelity F now becomes a plateau close to 1, as shown in Fig. 2(b). This is a sharp evidence for the existence of degenerate ground states and also rules out the multiple-transition scenario.

Generally, the two MPSs obtained from Random-DMRG and Boosted-DMRG are not orthogonal to each other and can be used to determine the two-dimensional ground-state subspace spanned by $|\Phi_\mathrm{I}\rangle$ and $|\tilde{\Phi}_\mathrm{I}\rangle$. This can be formulated as a variational problem by diagonalizing the Hamiltonian in this subspace, which yields two orthogonal states and their energies. For $-0.03 \leq J' \leq 0.08$, the relative difference between these two energies is smaller than 3×10^{-5} [74]. Also, we compute the energy variance $\sigma^2 \equiv \langle H^2\rangle - \langle H\rangle^2$ with respect to DMRG-optimized ground states and find that σ^2/N is smaller than 2×10^{-4}. Combining these observations with quasi-degenerate energy ($< 10^{-4}$), we conclude that the states obtained by Random- and Boosted-DMRG indeed form a two-dimensional ground-state space. It is also worth mentioning that the energy difference between these two states is smaller than the gap estimates in previous studies [30, 33].

Another essential signal of CSL around $J' = 0$ is that $|\Psi_\mathrm{S}\rangle$, the ground state in the semion sector, can be continuously evolved from $J' = 0.2$ to $J' = 0.02$ by using Boosted-DMRG. As shown in Fig. 2(c), the wave function fidelity between two neighboring-J' $|\Psi_\mathrm{S}\rangle$'s is always close to unit for $0.02 \leq J' \leq 0.2$, and the entanglement spectra of $|\Psi_\mathrm{S}\rangle$'s also show qualitative consistency in this region. Moreover, the tiny per-site energy variances of $|\Psi_\mathrm{S}\rangle$'s, $\sigma^2/N \sim 2.5\times10^{-4}$, further confirm that $|\Psi_\mathrm{S}\rangle$ is an eigenstate of Hamiltonian (1). It turns out that, when J' is closer and closer to $J' = 0$, the finite-size energy gap between identity and semion sectors becomes smaller and smaller, and meanwhile the edge semions at each boundary are more and more delocalized [74]. The decreasing energy gap cannot protect $|\Psi_\mathrm{S}\rangle$ anymore because of the numerical randomness introduced by DMRG, and two delocalized semions have more chance to "collide" with each other. Therefore, the breakdown of the evolution of $|\Psi_\mathrm{S}\rangle$ around $J' < 0.02$ is not an indication of a phase transition. Instead, it only suggests that the ground state in the semion sector cannot be stabilized by the DMRG calculations that naturally target the lowest energy state.

For the most contentious KHAF with $J' = 0$, we have also considered two more Gutzwiller ansätze associated with Eq. (2): (i) $[0,\pi]$ state [a gapless U(1) Dirac QSL] and (ii) $[0,0]$ state (a QSL with spinon Fermi surface) [38]. After converting them into MPSs, we find that their overlaps with the DMRG-optimized ground states are almost zero. When using these two ansätze for initializing DMRG, neither of them can improve the performance of DMRG. Although this does not rule out the U(1) Dirac and spinon Fermi surface QSL scenarios, it gives a hint that neither $[0,\pi]$ nor $[0,0]$ ansatz is a good description for the ground state of the KHAF.

Phase diagram. To investigate the nature of the other three phases for $J' \lesssim -0.04$, we calculate the NN spin-spin correla-

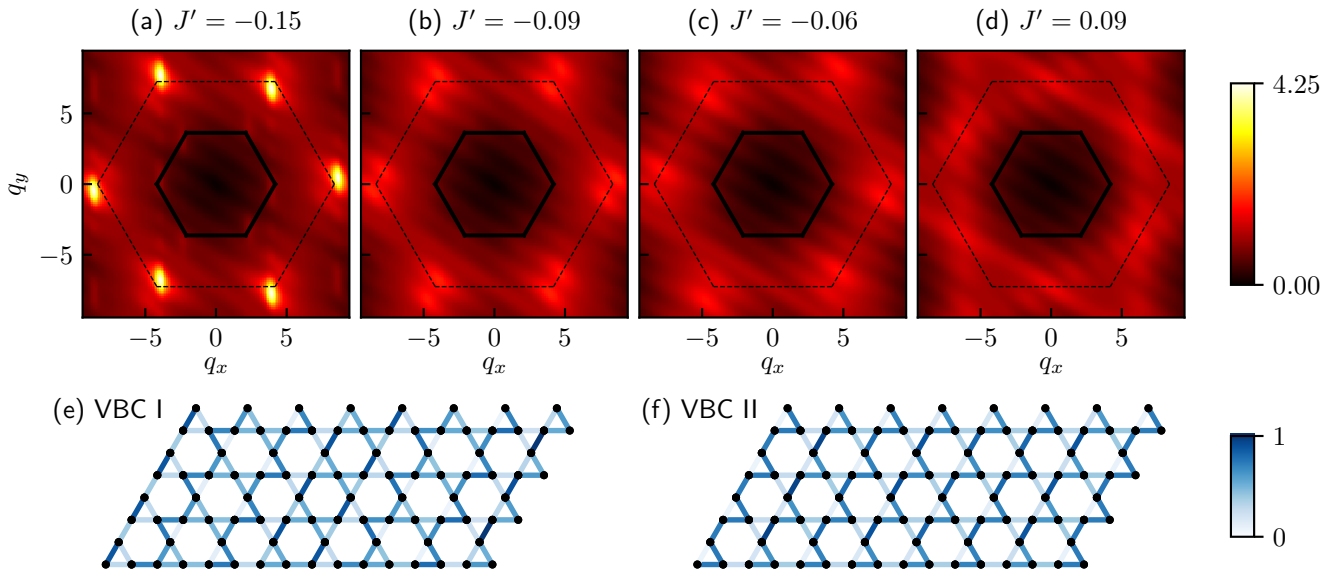

FIG. 3. Top: The spin structure factor $S(\mathbf{q})$ on 224-site YC8 cylinders for (a) the $\sqrt{3}\times\sqrt{3}$ phase, (b) the VBC I phase, (c) the VBC II phase, and (d) the CSL phase. The solid (dashed) hexagon is the first (extended) Brillouin zone of the kagome lattice. Bottom: Normalized absolute value of the NN spin-spin correlation $\langle \mathbf{S}_i \cdot \mathbf{S}_j \rangle$ on a 224-site YC8 cylinder for (e) the VBC I phase and (f) the VBC II phase. The cylinders are shown with only central columns.

tion $\langle \mathbf{S}_i \cdot \mathbf{S}_j \rangle$ and the spin structure factor

$$S(\mathbf{q}) = \frac{1}{N} \sum_{ij} \langle \mathbf{S}_i \cdot \mathbf{S}_j \rangle e^{i\mathbf{q}\cdot(\mathbf{r}_i - \mathbf{r}_j)} , \tag{4}$$

which are illustrated in Fig. 3. For $J' < -0.11$, $S(\mathbf{q})$ exhibits clear peaks at the K points in the extended Brillouin zone [see Fig. 3(a)], and the NN correlation $\langle \mathbf{S}_i \cdot \mathbf{S}_j \rangle$ is spatially uniform (not shown), which can be identified as the $\sqrt{3}\times\sqrt{3}$ spin-ordered phase [23, 31, 76]. In the two intermediate phases ($-0.11 \leq J' \leq -0.04$), $S(\mathbf{q})$ are featureless [see Figs. 3(b) and (c)], indicating the absence of long-range magnetic order, and the NN correlation $\langle \mathbf{S}_i \cdot \mathbf{S}_j \rangle$ exhibits clear translational symmetry breaking patterns [see Figs. 3(e) and (f)], which are two different VBC phases and dubbed as VBC I and VBC II in Fig. 1(a). Finally, in the CSL phase, $S(\mathbf{q})$ is featureless [see Fig. 3(d)] and the NN correlation $\langle \mathbf{S}_i \cdot \mathbf{S}_j \rangle$ is also spatially uniform (not shown), which are consistent with a QSL state.

Conclusion and discussion. To summarize, we revisit the KHAF by combining the DMRG method and analytical analyses and provide clear evidence that the CSL phase in the KHAF with longer-range interactions extends to a broader region in the phase diagram and, most strikingly, includes the KHAF with only NN interactions. In the vicinity of the CSL phase, two distinct VBC phases and a $\sqrt{3}\times\sqrt{3}$ magnetically ordered phase emerge in the phase diagram (in order of decreasing J').

Because of the breakdown of the adiabatic evolution of the semion sector around $J' < 0.02$, it is still hard to draw a solid conclusion on a gapped or gapless ground state at $J' = 0$. Thus, other TRS breaking states, e.g., a TRS breaking QSL with a Dirac node, can not be excluded at this elusive point.

Moreover, Gutzwiller projected wave function provides us a good initial ansatz to systematically prepare and study ground states in distinct topological sectors, without involving other technique tricks, such as pinning fields and flux insertion [54, 77]. Our work may also attract new future attention to this pendent issue. It would be desirable to observe the degenerate ground states at $J' = 0$ by, e.g., larger-scale DMRG calculations on wider cylinders or tensor network calculations in the thermodynamic limit. From the experimental side, the signature of semion excitations could be explored in real materials, even when the kagome compounds, having interactions beyond the KHAF with NN interactions, may no longer has a CSL as their ground states.

Acknowledgments. We thank Shou-Shu Gong, Ying-Hai Wu, Shuo Yang, Hong Yao, and Zheng Zhu for the valuable discussions. R.-Y.S. is supported by the COE research grant in computational science from Hyogo Prefecture and Kobe City through Foundation for Computational Science. H.-K.J. is funded by the European Research Council (ERC) under the European Unions Horizon 2020 research and innovation program (grant agreement No. 771537). H.-H.T. is supported by the Deutsche Forschungsgemeinschaft (DFG) through project A06 of SFB 1143 (project-id 247310070). Y.Z. is supported by National Natural Science Foundation of China (No.12034004 and No.11774306), the K. C. Wong Education Foundation (Grant No. GJTD-2020-01) and the Strategic Priority Research Program of Chinese Academy of Sciences (No. XDB28000000). The numerical simulations in this work are based on the GraceQ project [78].

* These two authors contributed equally.
† hong-hao.tu@tu-dresden.de
‡ yizhou@iphy.ac.cn

[1] P. W. Anderson, Mater. Res. Bull. **8**, 153 (1973).
[2] P. W. Anderson, Science **235**, 1196 (1987).
[3] P. A. Lee, Science **321**, 1306 (2008).
[4] L. Balents, Nature **464**, 199 (2010).
[5] L. Savary and L. Balents, Rep. Prog. Phys. **80**, 016502 (2016).
[6] Y. Zhou, K. Kanoda, and T.-K. Ng, Rev. Mod. Phys. **89**, 025003 (2017).
[7] J. Knolle and R. Moessner, Annu. Rev. Condens. Matter Phys. **10**, 451 (2019).
[8] C. Broholm, R. J. Cava, S. A. Kivelson, D. G. Nocera, M. R. Norman, and T. Senthil, Science **367** (2020).
[9] X. G. Wen, Phys. Rev. B **44**, 2664 (1991).
[10] M. B. Hastings, Phys. Rev. B **69**, 104431 (2004).
[11] V. Kalmeyer and R. B. Laughlin, Phys. Rev. Lett. **59**, 2095 (1987).
[12] V. Kalmeyer and R. B. Laughlin, Phys. Rev. B **39**, 11879 (1989).
[13] X. G. Wen, F. Wilczek, and A. Zee, Phys. Rev. B **39**, 11413 (1989).
[14] P. Mendels, F. Bert, M. A. de Vries, A. Olariu, A. Harrison, F. Duc, J. C. Trombe, J. S. Lord, A. Amato, and C. Baines, Phys. Rev. Lett. **98**, 077204 (2007).
[15] J. S. Helton, K. Matan, M. P. Shores, E. A. Nytko, B. M. Bartlett, Y. Yoshida, Y. Takano, A. Suslov, Y. Qiu, J.-H. Chung, D. G. Nocera, and Y. S. Lee, Phys. Rev. Lett. **98**, 107204 (2007).
[16] S.-H. Lee, H. Kikuchi, Y. Qiu, B. Lake, Q. Huang, K. Habicht, and K. Kiefer, Nat. Mater. **6**, 853 (2007).
[17] T.-H. Han, J. S. Helton, S. Chu, D. G. Nocera, J. A. Rodriguez-Rivera, C. Broholm, and Y. S. Lee, Nature **492**, 406 (2012).
[18] M. R. Norman, Rev. Mod. Phys. **88**, 041002 (2016).
[19] J. Marston and C. Zeng, J. Appl. Phys. **69**, 5962 (1991).
[20] R. R. P. Singh and D. A. Huse, Phys. Rev. B **76**, 180407 (2007).
[21] P. Nikolic and T. Senthil, Phys. Rev. B **68**, 214415 (2003).
[22] G. Evenbly and G. Vidal, Phys. Rev. Lett. **104**, 187203 (2010).
[23] S. Sachdev, Phys. Rev. B **45**, 12377 (1992).
[24] P. W. Leung and V. Elser, Phys. Rev. B **47**, 5459 (1993).
[25] P. Lecheminant, B. Bernu, C. Lhuillier, L. Pierre, and P. Sindzingre, Phys. Rev. B **56**, 2521 (1997).
[26] F. Mila, Phys. Rev. Lett. **81**, 2356 (1998).
[27] C. Waldtmann, H. U. Everts, B. Bernu, C. Lhuillier, P. Sindzingre, P. Lecheminant, and L. Pierre, Eur. Phys. J. B **2**, 501 (1998).
[28] P. Sindzingre and C. Lhuillier, EPL (Europhysics Letters) **88**, 27009 (2009).
[29] A. M. Läuchli, J. Sudan, and E. S. Sørensen, Phys. Rev. B **83**, 212401 (2011).
[30] A. M. Läuchli, J. Sudan, and R. Moessner, Phys. Rev. B **100**, 155142 (2019).
[31] A. Wietek and A. M. Läuchli, Phys. Rev. B **102**, 020411 (2020).
[32] H. C. Jiang, Z. Y. Weng, and D. N. Sheng, Phys. Rev. Lett. **101**, 117203 (2008).
[33] S. Yan, D. A. Huse, and S. R. White, Science **332**, 1173 (2011).
[34] S. Depenbrock, I. P. McCulloch, and U. Schollwöck, Phys. Rev. Lett. **109**, 067201 (2012).
[35] H.-C. Jiang, Z. Wang, and L. Balents, Nat. Phys. **8**, 902 (2012).
[36] S. Nishimoto, N. Shibata, and C. Hotta, Nat. Commun. **4**, 1 (2013).
[37] J.-W. Mei, J.-Y. Chen, H. He, and X.-G. Wen, Phys. Rev. B **95**, 235107 (2017).
[38] Y. Ran, M. Hermele, P. A. Lee, and X.-G. Wen, Phys. Rev. Lett. **98**, 117205 (2007).
[39] Y. Iqbal, F. Becca, S. Sorella, and D. Poilblanc, Phys. Rev. B **87**, 060405 (2013).
[40] Y. Iqbal, D. Poilblanc, and F. Becca, Phys. Rev. B **89**, 020407 (2014).
[41] Y. Iqbal, D. Poilblanc, and F. Becca, Phys. Rev. B **91**, 020402 (2015).
[42] Y.-C. He, M. P. Zaletel, M. Oshikawa, and F. Pollmann, Phys. Rev. X **7**, 031020 (2017).
[43] H. J. Liao, Z. Y. Xie, J. Chen, Z. Y. Liu, H. D. Xie, R. Z. Huang, B. Normand, and T. Xiang, Phys. Rev. Lett. **118**, 137202 (2017).
[44] S. S. Jahromi, R. Orús, D. Poilblanc, and F. Mila, SciPost Phys. **9**, 92 (2020).
[45] O. Götze, D. J. J. Farnell, R. F. Bishop, P. H. Y. Li, and J. Richter, Phys. Rev. B **84**, 224428 (2011).
[46] T. Li, (2018), arXiv:1807.09463.
[47] J. Thoenniss, M. K. Ritter, F. B. Kugler, J. von Delft, and M. Punk, (2020), arXiv:arXiv:2011.01268.
[48] K. Yang, L. K. Warman, and S. M. Girvin, Phys. Rev. Lett. **70**, 2641 (1993).
[49] L. Messio, B. Bernu, and C. Lhuillier, Phys. Rev. Lett. **108**, 207204 (2012).
[50] L. Messio, C. Lhuillier, and G. Misguich, Phys. Rev. B **87**, 125127 (2013).
[51] B. Bauer, L. Cincio, B. Keller, M. Dolfi, G. Vidal, S. Trebst, and A. W. W. Ludwig, Nat. Commun. **5**, 5137 (2014).
[52] A. Wietek, A. Sterdyniak, and A. M. Läuchli, Phys. Rev. B **92**, 125122 (2015).
[53] Y.-C. He, D. N. Sheng, and Y. Chen, Phys. Rev. Lett. **112**, 137202 (2014).
[54] S.-S. Gong, W. Zhu, and D. Sheng, Sci. Rep. **4**, 1 (2014).
[55] S.-S. Gong, W. Zhu, L. Balents, and D. N. Sheng, Phys. Rev. B **91**, 075112 (2015).
[56] W.-J. Hu, W. Zhu, Y. Zhang, S. Gong, F. Becca, and D. N. Sheng, Phys. Rev. B **91**, 041124 (2015).
[57] S. R. White, Phys. Rev. Lett. **69**, 2863 (1992).
[58] S. R. White, Phys. Rev. B **48**, 10345 (1993).
[59] U. Schollwöck, Ann. Phys. **326**, 96 (2011).
[60] X. G. Wen, Phys. Rev. B **44**, 2664 (1991).
[61] X.-G. Wen, Phys. Lett. A **300**, 175 (2002).
[62] X.-G. Wen, Phys. Rev. B **65**, 165113 (2002).
[63] Y. Zhou and X.-G. Wen, arXiv **cond-mat/0210662** (2002), 10.48550/ARXIV.COND-MAT/0210662.
[64] Other parton ansätze in this Letter will be labeled in the same scheme.
[65] Y. Zhang, T. Grover, A. Turner, M. Oshikawa, and A. Vishwanath, Phys. Rev. B **85**, 235151 (2012).
[66] H.-H. Tu, Y. Zhang, and X.-L. Qi, Phys. Rev. B **88**, 195412 (2013).
[67] Y.-H. Wu, L. Wang, and H.-H. Tu, Phys. Rev. Lett. **124**, 246401 (2020).
[68] H.-K. Jin, H.-H. Tu, and Y. Zhou, Phys. Rev. B **101**, 165135 (2020).
[69] H.-K. Jin, H.-H. Tu, and Y. Zhou, Phys. Rev. B **104**, L020409 (2021).
[70] J.-Y. Chen, J.-W. Li, P. Nataf, S. Capponi, M. Mambrini, K. Totsuka, H.-H. Tu, A. Weichselbaum, J. von Delft, and D. Poilblanc, Phys. Rev. B **104**, 235104 (2021).
[71] H. Li and F. D. M. Haldane, Phys. Rev. Lett. **101**, 010504 (2008).

[72] X.-L. Qi, H. Katsura, and A. W. W. Ludwig, Phys. Rev. Lett. **108**, 196402 (2012).
[73] R.-Y. Sun and Z. Zhu, Phys. Rev. B **104**, L121118 (2021).
[74] See the Supplemental Material for more details.
[75] DMRG is typically biased towards a low-entanglement combination. Here, however, the state is an equal weight superposition of two minimally entangled states, i.e., $(e^{i\theta}|\Psi_1\rangle + e^{-i\theta}|\Psi_1{}^*\rangle)/\sqrt{2}$, which DMRG has no preference over a particular θ.
[76] F. Kolley, S. Depenbrock, I. P. McCulloch, U. Schollwöck, and V. Alba, Phys. Rev. B **91**, 104418 (2015).
[77] Y.-C. He, D. N. Sheng, and Y. Chen, Phys. Rev. B **89**, 075110 (2014).
[78] GraceQ, www.gracequantum.org.

Supplemental Material for "Possible chiral spin liquid state in the $S = 1/2$ kagome Heisenberg model"

This Supplemental Material includes more numerical details about energetic comparison between Random-DMRG and Boosted-DMRG, chirality estimation in the CSL phase, finite-size gaps between two topological sectors, and edge spinons in the semion sector.

Ground-state energy comparisons and re-diagonalization

We first introduce the relative energy difference between two close energies, E_1 and E_2, as

$$\delta(E_1, E_2) \equiv \left| \frac{E_1 - E_2}{(E_1 + E_2)/2} \right| . \tag{S1}$$

TABLE S1. Relative energy difference between Random-DMRG and Boosted-DMRG states, $\delta(E_{\rm RD}, E_{\rm BD})$, and between two re-orthogonalized states, $\delta(\tilde{E}_1, \tilde{E}_2)$, in the CSL phase on a 224-site YC8 cylinder.

J'	$\delta(E_{\rm RD}, E_{\rm BD})$	$\delta(\tilde{E}_1, \tilde{E}_2)$
0.08	1.81×10^{-9}	3.13×10^{-7}
0.07	1.92×10^{-7}	2.39×10^{-6}
0.06	1.50×10^{-7}	2.44×10^{-6}
0.05	9.96×10^{-8}	1.92×10^{-6}
0.04	1.35×10^{-7}	4.73×10^{-6}
0.03	9.97×10^{-9}	2.82×10^{-5}
0.02	1.72×10^{-7}	4.11×10^{-6}
0.01	1.29×10^{-7}	3.44×10^{-6}
0	6.45×10^{-8}	1.13×10^{-5}
-0.01	4.42×10^{-7}	9.79×10^{-7}
-0.02	1.61×10^{-6}	2.63×10^{-6}
-0.03	1.49×10^{-6}	4.90×10^{-6}

As mentioned in the main text, we obtained two almost degenerate ground states, $|\Psi_{\rm RD}\rangle$ and $|\Psi_{\rm BD}\rangle$, by using Random-DMRG and Boosted-DMRG, respectively. In the CSL phase, these two states are generally not orthogonal to each other. Denoting the variational energy of $|\Psi_{\rm RD}\rangle$ ($|\Psi_{\rm BD}\rangle$) as $E_{\rm RD}$ ($E_{\rm BD}$), the relative energy difference $\delta(E_{\rm RD}, E_{\rm BD})$ is extremely small, as listed in Table S1.

With two non-orthogonal MPSs $|\Psi_{\rm RD}\rangle$ and $|\Psi_{\rm BD}\rangle$ in hand, we carry out a further variational optimization to obtain re-orthogonalized states and corresponding energies. This optimization is formulated as a generalized eigenvalue problem by contructing the following 2×2 matrices:

$$H_2 = \begin{pmatrix} \langle\Psi_{\rm RD}|H|\Psi_{\rm RD}\rangle & \langle\Psi_{\rm RD}|H|\Psi_{\rm BD}\rangle \\ \langle\Psi_{\rm BD}|H|\Psi_{\rm RD}\rangle & \langle\Psi_{\rm BD}|H|\Psi_{\rm BD}\rangle \end{pmatrix}, \tag{S2}$$

and

$$N_2 = \begin{pmatrix} \langle\Psi_{\rm RD}|\Psi_{\rm RD}\rangle & \langle\Psi_{\rm RD}|\Psi_{\rm BD}\rangle \\ \langle\Psi_{\rm BD}|\Psi_{\rm RD}\rangle & \langle\Psi_{\rm BD}|\Psi_{\rm BD}\rangle \end{pmatrix}. \tag{S3}$$

By solving the generalized eigenvalue problem, namely, $H_2 x = E N_2 x$, we can obtain two re-diagonalized eigenenergies, $\tilde{E}_1$ and $\tilde{E}_2$. The relative energy difference $\delta(\tilde{E}_1, \tilde{E}_2)$, with respect to newly obtained $\tilde{E}_1$ and $\tilde{E}_2$, is listed in Table S1.

Spin chirality

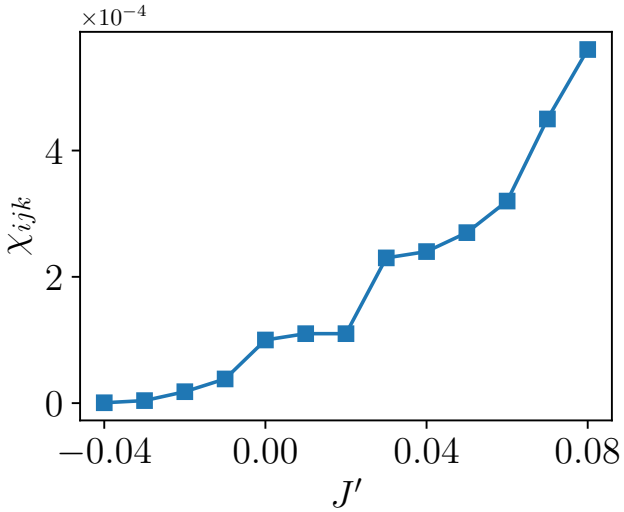

FIG. S1. χ_{ijk} on an elementary triangle in the center of a 224-site YC8 cylinder as a function of J'.

In order to characterize the chirality, we define the three-spin operator on an elementary triangle $\triangle_{ijk}$ [see the elementary triangles in Fig. 1(b)] as

$$E_{ijk} = \mathbf{S}_i \cdot \left(\mathbf{S}_j \times \mathbf{S}_k \right). \tag{S4}$$

Notice that E_{ijk} is purely imaginary and Hermitian, indicating that $\langle\psi|E_{ijk}|\psi\rangle = 0$ for any real state $|\psi\rangle$.

In the CSL phase, we can obtain two orthogonal degenerate ground states, $|\tilde{\Phi}_1\rangle$ and $|\tilde{\Phi}_2\rangle$, by the re-diagonalization method introduced above. Because both $|\tilde{\Phi}_1\rangle$ and $|\tilde{\Phi}_2\rangle$ are real wave functions, the expectation values of E_{ijk} with respect to those two states must be zero. Nevertheless, we can evaluate the spin chirality by introducing the following 2×2 matrix:

$$\chi_2(ijk) = \begin{pmatrix} 0 & \langle\tilde{\Phi}_1|E_{ijk}|\tilde{\Phi}_2\rangle \\ \langle\tilde{\Phi}_2|E_{ijk}|\tilde{\Phi}_1\rangle & 0 \end{pmatrix}. \tag{S5}$$

It is easy to verify that $\chi_2(ijk)$ is Hermitian and has symmetric eigenvalues with respect to zero, namely, $\pm\chi_{ijk}$ ($\chi_{ijk} > 0$), corresponding to chiral and anti-chiral ground states, respectively. Hereafter we choose the elementary triangle $\triangle_{ijk}$ in the center of a YC8 cylinder to compute χ_{ijk}. Notice that there are two types of elementary triangles corresponding to up- and down-triangles and they give rise to almost the same results. For relatively large J' ($J' = 0.2$), we find that $\chi_{ijk} \approx 0.06$ which is very close to the result obtained in Ref. [55]. As

shown in Fig. S1, χ_{ijk} decreases as J' decreases. At the point of $J' = 0$, we find that $\chi_{ijk} \approx 1.0 \times 10^{-4}$, and at the transition point between the VBC II and CSL phases ($J' = -0.04$), $\chi_{ijk} \approx 6.0 \times 10^{-7}$ is almost zero.

Finite-size gap between identity and semion sectors

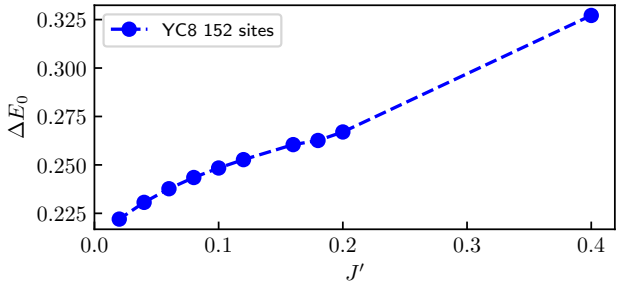

FIG. S2. The finite energy gaps between $|\Psi_I\rangle$ and $|\Psi_S\rangle$ on a 152-site YC8 cylinder.

Although the ground states in the identity and semion sectors, namely, $|\Psi_I\rangle$ and $|\Psi_S\rangle$, are degenerate in the thermodynamic limit, a finite energy gap between these two states always exists in finite-size systems. In Fig. S2, we show that this finite-size gap decreases with J' in the regime of $0.02 \leq J' \leq 0.4$.

Localization length of the edge semions

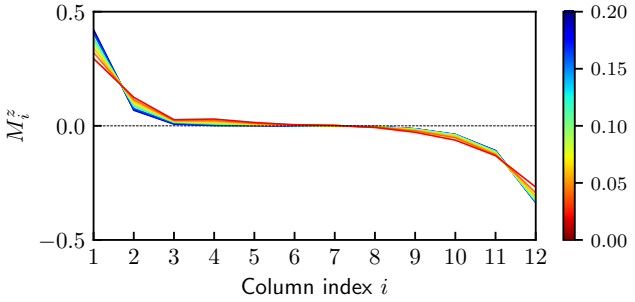

FIG. S3. The evolution of the column summation of the M_i^z distribution of semion sector states in the 152-site YC8 system from $J' = 0.2$ to $J' = 0.02$. The coupling J' for each curve can be read from the colorbar.

For the ground state in the semion sector, we measure the total magnetization on the i-th column, M_i^z, as

$$M_i^z = \sum_j \langle \Psi_S | S_{i,j}^z | \Psi_S \rangle, \tag{S6}$$

where i and j are column and row indices, respectively, and the summation $\sum_j$ runs over all the lattice sites belonging to the i-th column. In Fig. S3, we show the M_i^z profile for various J'. Clearly, the localization lengths of two semions at the boundaries of the cylinder increase as J' decreases, from which it is expected that the localization length of each edge semion might be as large as half of the cylinder length when J' is close to $J' = 0$.